THE JOURNAL OF PHYSICAL CHEMISTRY C

Article

Cite This: J. Phys. Chem. C 2018, 122, 21724−21734

pubs.acs.org/JPCC

Impedance Resonance in Narrow Confinement

Sonja Babel,[†] Michael Eikerling,[‡] and Hartmut Löwen*[,†]

[†]Institut für Theoretische Physik II: Weiche Materie, Heinrich-Heine-Universität Düsseldorf, Universitätsstraße 1, D-40225 Düsseldorf, Germany

[‡]Department of Chemistry, Simon Fraser University, 8888 University Drive, Burnaby, British Columbia, Canada V5A 1S6

Supporting Information

ABSTRACT: The article explores the ion flux response of a capacitor configuration to an alternating voltage. The model system comprises a symmetric binary electrolyte confined between plan-parallel capacitor plates. The alternating current response is investigated for the sparsely studied albeit practically important case of a large amplitude voltage applied across a narrow capacitive device, with the distance between the two plates amounting to a few ion diameters. Dynamic density functional theory is employed to solve for the spatiotemporal ion density distribution as well as the transient ion flux and complex impedance of the system. The analysis of these properties reveals a hitherto hidden impedance resonance. A single ion analogue of the capacitor, which is equivalent to neglecting all interactions between the ions, is employed for a physical interpretation of this phenomenon. It explains the resonance as a consequence of field-induced ion condensation at the capacitor plates and coherent motion of condensed ions in response to the field variation.

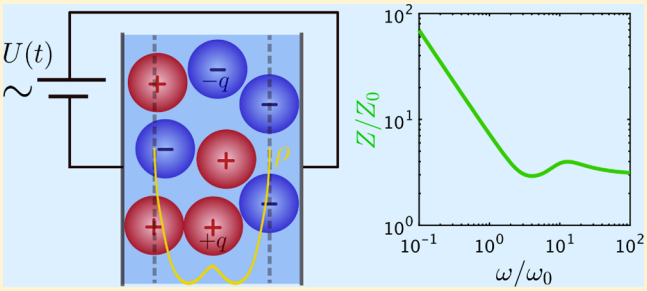

INTRODUCTION

There is a growing interest in understanding capacitive phenomena in narrowly confined ionic systems.[1−4] Obviously, the topic is of fundamental importance in electrochemistry. Besides, it is of practical utility for analyzing the dynamic response of charged colloidal systems[5−7] as well as nanoelectrochemical systems[8,9] to a varying electric field, as encountered for instance in electroactuators[10,11] or capacitive deionization systems.[12−14] The size of ions in relation to the size of the confining systems is a crucial consideration in such systems. Specifically, for ionic systems confined to lengths on the order of the ion diameter, steric effects become important.

The archetypal capacitive system consists of a liquid electrolyte or ionic liquid that is confined by rigid walls made of a metallic conductor insulated against the electrolyte, as depicted in Figure 1. The model system used here is infinite in lateral direction, rendering the problem effectively one-dimensional. Note that there is thus no bulk from which ions are taken or to which ions can leave nor are charges transferred from the ions to the walls. Ions only move back and forth within the gap. The primordial scientific interest lies in understanding the response of such a system to a modulation of the applied metal-phase potential, which is a topic of central interest in physical chemistry. The response function in question is the result of a complex interplay between variations in metal surface charge density, electrolyte potential, and ion density distribution.

In this work, classical dynamic density functional theory (DDFT)[15−18] is used to study the ion dynamics in a narrow electrolyte slab, whose thickness equals a few ionic diameters. The ionic system is exposed to a dynamic voltage between the capacitor plates with harmonic (sinusoidal) time dependence determined by the angular frequency ω and the amplitude ΔU.

The motivation to study this model is threefold: first of all, the model is best applied to the mesoscopic scale for oppositely charged colloids.[5,6] Using organic solvents, these can be prepared even at low concentrations of dissolved ionic countercharges such that the microion concentration is small.[19] These dispersions have been exposed to direct current[20] and alternating current (AC)[21] electric fields that gave rise to strong spatiotemporal responses. The presented model system resembles the configuration considered in ref 21 though in our case the electrolyte-filled slit between the walls is only a few colloidal layers wide. Apparent issues in applying our model to colloids lie in ignoring the residual microion concentration, which however can be kept to small (micromolar) concentrations in organic solvents, and neglecting the hydrodynamic interactions mediated by the solvent, which can be justified by using particles whose hydrodynamic radius is much smaller than their interaction radius, as is the case for solvent-permeable particles.[22,23] The mentioned problems are also mitigated by the fact that the responses of the microions and solvent molecules on the one hand and the colloidal ions on the other hand are separated in the frequency domain. The colloidal system can of course be scaled down in size toward charged micelles and nanocolloids.

Received: June 11, 2018
Revised: September 4, 2018
Published: September 5, 2018

DOI: 10.1021/acs.jpcc.8b05559
J. Phys. Chem. C 2018, 122, 21724−21734

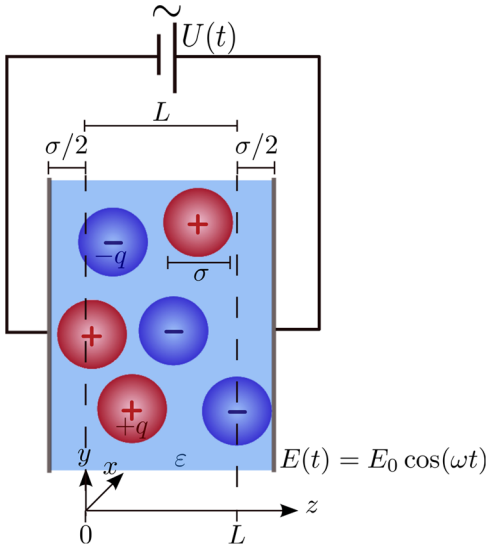

Figure 1. Sketch of the system. Balanced numbers of equally sized ions with diameter σ and charge $q_\pm = \pm q$ are kept in a slab between two plan-parallel insulating capacitor plates in an electrolyte of relative dielectric constant ε. The width L denotes the accessible length in z-direction. For simplicity, the system is assumed to be infinitely extended in xy-direction. An alternating external voltage $U(t)$ with amplitude ΔU produces an oscillating electric field $E(t)$ acting on the ions.

Secondly, one can think about a molecular realization in nanogap electrodes with the capacitor walls electrically isolated from the electrolyte in order to prevent any ion oxidation at the walls. The peculiar geometry has not yet been exploited experimentally but is in principle feasible.[24] It should be noted though that applying our model to this case implies neglecting any specific solvent contributions to the AC electric field response as well as any structural details of the walls.[25]

Thirdly, the considered model logically extends basic model studies of capacitor configurations that can be traced back to classical works of Gouy (1910)[26] and Chapman (1913).[27] From these early works, problems of electrified interfaces and confined electrolytes were approached using continuum theories based on Poisson−Boltzmann and Poisson−Nernst−Planck (PNP) equations. Later on, these continuum theories were modified to account for steric effects induced by finite ion size[28−36] and specific solvent polarization effects.[37]

Our model system is similar to those considered in recent theoretical studies by Beunis et al.,[38] Olesen et al.,[39] and Feicht et al.[40] However, in contrast to those works, we consider a case of more narrow ion confinement, wherein the width of the electrolyte slab, L, is on the order of several ion diameters, σ, that is, $\sigma \leq L \leq 4\sigma$, and we focus entirely on the limit of large electric fields. We employ classical dynamic density functional theory[15−18] (DDFT), including the steric repulsion between the ions. A similar model has been used before in refs 35, 36 to consider the charging kinetics of an electric double layer in response to a voltage step.

Here, we apply this approach to study the capacitive response of the ionic system to a transient electric field. Our system is smaller than the one that was considered in refs 35, 36, and we are interested in the ion flux response to an AC voltage signal with large amplitude. This response function should be amenable to experimental study by electrochemical impedance spectroscopy.

DDFT is known to be computationally highly efficient and it allows geometric parameters like ion diameter and slab thickness to be tuned widely. With DDFT, the system response can be studied under large amplitude, $\Delta U \gg U_T$, with the thermal voltage $U_T = k_B T/q$, where k_B is the Boltzmann constant, T is the temperature, and q is the ion charge, and over a wide range of ω. It is thus an ideal tool to explore ion dynamics in a capacitor configuration in the limit of strong ion confinement[1−4] where the full interplay of steric correlation effects, electrostatic interactions, as well as ion transport by diffusion and migration unfolds.

In the following section, we introduce the model system and describe the physical-computational methodology based on dynamic density functional theory. Equations are non-dimensionalized and typical parameter sets are discussed. In the results section, we analyze and discuss the dynamic density profiles of ions and the impedance response of the microscopic model system. A single-ion capacitor model is presented to explain the observed resonance effect in the impedance.

MODEL

An electroneutral mixture of colloidal cations and anions with equal charge magnitude q and equal diameter σ is kept in a stagnant fluid with dielectric constant ε. This ionic system[30,41−49] is confined between two infinitely extended plan-parallel capacitor plates;[38−40,50−56] see Figure 1. The plates are polarized with an external alternating voltage $U(t)$ that creates an oscillating electric field $E(t)$ across the electrolyte slab. The ions are modeled within the restricted primitive model[57−66] as hard charged spheres of diameter σ interacting via steric and Coulomb interactions. The capacitor plates are introduced as hard insulating walls leading to a no-flow condition for the ions. The outermost possible position of the ion centers is then situated at a distance $\sigma/2$ away from the physical walls. L denotes the accessible width perpendicular to the capacitor plates. The system is considered in the highly confined limit where L is on the order of σ.

We solve the model for the time- and space-dependent densities of the two ion species using DDFT,[15−18] which is the time-dependent variant of classical DFT.[67−79] From the densities, we also obtain the charge flux in the system. The linear response part of the current is used to further calculate a quantity that is analogous to a local impedance of the capacitor configuration. Subsequently, we will therefore refer to it as the local impedance.

Theory. *Dynamic Density Functional Theory (DDFT).* Dynamic density functional theory relates the time evolution of the density to the functional derivative of the free energy of the system in the form

$$\frac{\partial \rho_\pm(\vec{r}, t)}{\partial t} = \beta D \nabla \left[\rho_\pm(\vec{r}, t) \nabla \left(\frac{\delta \mathcal{F}[\rho_+(\vec{r}, t), \rho_-(\vec{r}, t)]}{\delta \rho_\pm(\vec{r}, t)} \right) \right] \tag{1}$$

where $\rho_\pm(\vec{r}, t)$ stands for the density of the ions with either positive ρ_+ or negative charge ρ_- as a function of position $\vec{r}$ and time t; $\beta = 1/k_B T$ is the inverse thermal energy, and D is the diffusion coefficient of the ions, which, for simplicity, is taken to be the same for both ion species $D_+ = D_- \equiv D$. $\mathcal{F}$ denotes the free energy of the system, which is a functional of the two densities ρ_+ and ρ_-, and $\frac{\delta}{\delta \rho_\pm}$ is the functional derivative[80,81] with respect to the density. By connecting the time derivative

DOI: 10.1021/acs.jpcc.8b05559
J. Phys. Chem. C 2018, 122, 21724−21734

of the density to the functional derivative of the system's energy, DDFT shifts the problem of determining the time evolution of the densities to the problem of knowing the energy of the system for any given density distribution. If we know the energy of all states, we can determine the time evolution of the system from this knowledge. Thus, we first need to construct an expression for the energy of the system. We consider a free energy functional of the form

$$\mathcal{F} = \mathcal{F}^{\mathrm{id}} + \mathcal{F}^{\mathrm{HS}} + \mathcal{F}^{\mathrm{Coul}} + \int \mathrm{d}\vec{r}\, \rho_{\pm}(\vec{r}, t) V_{\mathrm{ext},\pm}(\vec{r}, t) \tag{2}$$

The ideal part $\mathcal{F}^{\mathrm{id}}$ gives the free energy of an ideal gas. The remaining terms describe the interaction of the particles due to steric hard-sphere $\mathcal{F}^{\mathrm{HS}}$ and charge effects $\mathcal{F}^{\mathrm{Coul}}$ (Coulomb) as well as the effect of the external potential $V_{\mathrm{ext},\pm}(\vec{r}, t) = -q_{\pm}E(t)z$ with the electric field

$$E(t) = E_0 \cos(\omega t) \tag{3}$$

The amplitude E_0 is related to the voltage amplitude ΔU and the accessible system length L by

$$E_0 = \Delta U / L \tag{4}$$

The ideal part $\mathcal{F}^{\mathrm{id}}$ is known exactly, the hard-sphere (HS) part is described by fundamental measure theory (FMT),[14,82−86] introduced in the next paragraph, while the Coulomb interaction is taken into account with a mean-field approach,[56,85] such that for the ions within a volume V we obtain

$$\begin{aligned}
\mathcal{F}^{\mathrm{id}}[\rho_+, \rho_-] &= k_{\mathrm{B}}T \sum_{\pm} \int_V \mathrm{d}\vec{r} \rho_{\pm}(\vec{r}, t) \ln(\Lambda^3 \rho_{\pm}(\vec{r}, t)) \\
\mathcal{F}^{\mathrm{HS}}[\rho_+, \rho_-] &= \mathcal{F}^{\mathrm{FMT}}[\rho_+ + \rho_-] \\
\mathcal{F}^{\mathrm{Coul}}[\rho_+, \rho_-] &= \frac{1}{8\pi\epsilon\epsilon_0} \int_V \mathrm{d}\vec{r} \int_V \mathrm{d}\vec{r}' \frac{\rho_{\mathrm{c}}(\vec{r}, t)\rho_{\mathrm{c}}(\vec{r}', t)}{|\vec{r} - \vec{r}'|}
\end{aligned} \tag{5}$$

with charge density $\rho_{\mathrm{c}}(\vec{r}, t) = q(\rho_+(\vec{r}, t) - \rho_-(\vec{r}, t))$. ε_0 denotes the vacuum and ε denotes the relative permittivity. Λ is the de Broglie wavelength. As a remark, an extension of this functional to account for short-range electrostatic correlations between the ions was recently derived in ref 74.

Fundamental Measure Theory (FMT). We use the White Bear II version of the fundamental measure theory in tensor[87] form[84,85] to write the hard-sphere contribution to the free energy functional as

$$\mathcal{F}^{\mathrm{FMT}} = \int_V \mathrm{d}\vec{r}\, \Phi(\{n_\alpha\}) \tag{6}$$

where $\Phi = \Phi_1 + \Phi_2 + \Phi_3$ is the free energy density with

$$\begin{aligned}
\Phi_1 &= -\frac{n_2}{4\pi R^2} \ln(1 - n_3) \\
\Phi_2 &= \frac{1}{4\pi R}(n_2^2 - \vec{n}_2 \cdot \vec{n}_2) \frac{1 + \frac{1}{3}\psi_2(n_3)}{1 - n_3} \\
\Phi_3 &= \left(n_2^3 - 3n_2 \vec{n}_2 \cdot \vec{n}_2 + \frac{9}{2}(\vec{n}_2 \vec{n}_{m_2} \vec{n}_2 - \mathrm{Tr}(\vec{n}_{m_2}^3))\right) \\
&\quad \times \frac{1 - \frac{1}{3} n_3 \psi_3(n_3)}{24\pi(1 - n_3)^2}
\end{aligned} \tag{7}$$

using the functions

$$\begin{aligned}
\psi_2 &= \frac{1}{n_3}(2n_3 - n_3^2 + 2(1 - n_3)\ln(1 - n_3)) \\
\psi_3 &= \frac{1}{n_3^2}(2n_3 - 3n_3^2 + 2n_3^3 + 2(1 - n_3)^2 \ln(1 - n_3))
\end{aligned} \tag{8}$$

These expressions are solely dependent on a set of functions n_ω referred to as weighted densities, which are obtained from convolutions of the particle density ρ with weight functions $\omega^{(\alpha)}$ such that

$$n_\alpha(\vec{r}, t) = \int_V \rho(\vec{r}', t) \omega^{(\alpha)}(\vec{r} - \vec{r}') \mathrm{d}\vec{r}' \tag{9}$$

where

$$\begin{aligned}
\omega^{(2)}(\vec{r}) &= \delta(R - |\vec{r}|) \\
\omega^{(3)}(\vec{r}) &= \theta(R - |\vec{r}|) \\
\vec{\omega}^{(2)}(\vec{r}) &= \frac{\vec{r}}{|\vec{r}|}\delta(R - |\vec{r}|) \\
\overleftrightarrow{\omega}^{(m_2)}(\vec{r}) &= \left(\frac{\vec{r} \cdot \vec{r}^{\,t}}{|\vec{r}|^2} - \frac{\overleftrightarrow{\mathbb{I}}}{3}\right)\delta(R - |\vec{r}|)
\end{aligned} \tag{10}$$

are the weights in the case of spherical particles. Here, $R = \sigma/2$ denotes the hard-sphere radius. δ is the Dirac delta function, θ is the heavyside step function, $\vec{r}^{\,t}$ is the transpose of the vector $\vec{r}$, and $\overleftrightarrow{\mathbb{I}}$ is the unit matrix. Arrows indicate vectors, while the double-headed arrow denotes a matrix. Tr in eq 7 is the trace of the matrix, that is, the sum of its diagonal elements. In particular, the weighted density $n_3(\vec{r}, t)$ gives the number of particles within a sphere of radius R around $\vec{r}$ at time t. Term Φ_1 of eq 7 ensures, via divergence of the logarithm, that this value does not become unphysical, that is, larger than one, thus accounting for the particle size.

System Parameters and Nondimensionalization. We will present parameterizations for the model on two different length scales. For a microscale realization, we consider low-charged colloidal particles of charge $q = |q_{\pm}| = 5e$, where e is the elementary charge, and of diameter $\sigma = 2.61\ \mu$m, which serves as the length scale. We further assume the ions to be partially solvent permeable with a hydrodynamic radius of $R_{\mathrm{h}} = \frac{\sigma}{20}$. The relative permittivity of the organic electrolyte is assumed as $\varepsilon = 2.3$, corresponding for instance to the relative permittivity of a decalin−tetrachloroethylene mixture as discussed in ref 88. The energy scale is set by the thermal energy at standard temperature ($T = 298$ K), $k_{\mathrm{B}}T = 4.11 \times 10^{-21}$ J, that can be used to define a thermal voltage $U_{\mathrm{T}} = k_{\mathrm{B}}T/$

DOI: 10.1021/acs.jpcc.8b05559
J. Phys. Chem. C 2018, 122, 21724−21734

Table 1. Summary of the System Parameters[a]

dimensional property	symbol	definition	normalized value	typical value nanoscale	typical value microscale
ion diameter	σ		1	3 nm	2.61 μm
accessible system length	L		L/σ	10 nm	8.70 μm
Bjerrum length	λ_B	$q^2/(4\pi\epsilon\epsilon_0 k_B T)$	$q^2/(4\pi\epsilon\epsilon_0 k_B T\sigma)$	0.70 nm	0.61 μm
Debye length	λ_D	$\frac{\sigma}{2}\sqrt{\frac{\sigma}{\lambda_B}\frac{1}{6\phi}}$	$\frac{1}{2}\sqrt{\frac{\sigma}{\lambda_B}\frac{1}{6\phi}}$	2.07 nm	1.80 μm
self-diffusion time	τ_0	σ^2/D_0	1	5.50×10^{-8} s	5.25 s
driving period	T		TD_0/σ^2		
transit time	τ_{tr}	$\pi L^2 k_B T/(2qUD_0)$	$\pi L^2/(2\sigma^2 U^*)$	2.47×10^{-9} s	2.35 s
diffusion time	τ_{diff}	L^2/D_0	L^2/σ^2	6.12×10^{-7} s	58.3 s
self-diffusion frequency	ω_0	$2\pi D_0/\sigma^2$	2π	1.14×10^{8} s^{-1}	1.20 s^{-1}
driving frequency	ω		$\omega\sigma^2/2\pi D_0$		
transit frequency	ω_{tr}	$4qUD_0/(L^2 k_B T)$	$4\sigma^2 U^*/L^2$	2.54×10^{9} s^{-1}	2.67 s^{-1}
diffusion frequency	ω_{diff}	$2\pi D_0/L^2$	$2\pi\sigma^2/L^2$	1.03×10^{8} s^{-1}	0.11 s^{-1}
current scale	j_0	$q/(\sigma^2\tau_0)$	1	3.23×10^{5} A m^{-2}	2.24×10^{-8} A m^{-2}
current harmonics	j_n	$\frac{2}{T}\int_{-T/2}^{T/2} dt\, j(\vec{r}, t)\, e^{-in\omega t}$	j_n/j_0		
thermal voltage	U_T	$k_B T/q$	1	25.7 mV	5.14 mV
external voltage	ΔU	$\Delta U = E_0 L$	$\Delta U/U_T = U^*$	1 V	0.2 V
impedance scale	Z_0	$k_B T\tau_0/q^2$	1	8.8×10^{9} Ω	3.36×10^{16} Ω
impedance	Z	$U/(j_1\sigma^2)$	$U^* j_0/j_1$		
relative permittivity	ϵ			80	2.3
particle charge	q		q/e	1e	5e

[a]Typical values are given for the two possible realizations constituted by a system of relatively large monovalent ions (nanoscale) with L = 10 nm, σ = 3 nm, $q = e$, $D_0 = 1.63 \times 10^{-10}$ m^2 s^{-1}, $k_B T = 4.11 \times 10^{-21}$ J, and ΔU = 1.0 V and a system of low-charged partially solvent-permeable colloidal particles (microscale) where L = 8.70 μm, σ = 2.61 μm, $q = 5e$, $D_0 = 1.30 \times 10^{-12}$ m^2 s^{-1}, $k_B T = 4.11 \times 10^{-21}$ J, and ΔU = 0.2 V, both leading to the same normalized system parameters.

q = 5.14 mV. The viscosity of the electrolyte at room temperature is $\eta = 1.29 \times 10^{-3}$ Pa s, such that the diffusion constant of macroions is $D_0 = \frac{k_B T}{6\pi\eta R_h} = 1.30 \times 10^{-12}$ m^2 s^{-1}. We define a characteristic time scale $\tau_0 = \sigma^2/D_0 = 5.25$ s that corresponds to a characteristic angular frequency $\omega_0 = \frac{2\pi}{\tau_0} = 1.20$ s^{-1}.

On the other hand, a nanoscale system of monovalent ions at the same temperature with $q = e$, σ = 2, R_h = 3 nm, ϵ = 80, and $U_T = k_B T/q$ = 25.7 mV leads to the same reduced system parameters. With the viscosity of water at room temperature, $\eta_{water} = 8.9 \times 10^{-4}$ Pa s, the diffusion coefficient in this case is $D_0 = 1.63 \times 10^{-10}$ m^2 s^{-1} and the time and frequency scales are now given by $\tau_0 = 5.5 \times 10^{-8}$ s and $\omega_0 = 1.14 \times 10^{8}$ s^{-1}, respectively. The following calculation can thus be considered in either of these cases. A summary of the system parameters can be found in Table 1.

The dimensionless amplitude of the applied voltage is given by

$$U^* = \frac{\Delta U}{U_T} \tag{11}$$

As a baseline parameter for this amplitude, we use U^* = 38.9.

In addition to the ion diffusion and self-diffusion time, $\tau_{diff} = \frac{L^2}{D_0}$ and $\tau_0 = \frac{\sigma^2}{D_0}$, respectively, we introduce the ion transit time, τ_{tr}, which corresponds to the time that an ion needs to cross the thickness of the device when the electric field is not screened. The latter is given by the ratio of the system length L and the mean velocity of the particles in the unscreened case, $\overline{v} = \frac{qE}{\gamma}\frac{2}{T}\int_{-T/4}^{T/4} dt\, \cos(\omega t) = \frac{2}{\pi}\frac{U^* D}{L}$, as $\tau_{tr} = \frac{L}{\overline{v}} = \frac{\pi}{2}\frac{U_T}{\Delta U}\frac{L^2}{D_0}$. All time scales are normalized to the self-diffusion time τ_0, such that the dimensionless ion transit time becomes

$$\frac{\tau_{tr}}{\tau_0} = \frac{\pi}{2}\frac{L^2}{\sigma^2 U^*} \tag{12}$$

and the dimensionless diffusion time of ions in the electrolyte is

$$\frac{\tau_{diff}}{\tau_0} = \frac{L^2}{\sigma^2} \tag{13}$$

The corresponding dimensionless angular frequencies are given by

$$\frac{\omega_{tr}}{\omega_0} = \frac{2}{\pi}\frac{U^*\sigma^2}{L^2} \tag{14}$$

and

$$\frac{\omega_{diff}}{\omega_0} = \frac{\sigma^2}{L^2} \tag{15}$$

The free parameters of the model, varied in simulations, are ΔU and L.

The dimensionless thickness L/σ should be evaluated in relation to two common characteristic length scales of ionic systems: Bjerrum length λ_B and Debye length λ_D, which are given in the dimensionless form as

DOI: 10.1021/acs.jpcc.8b05559
J. Phys. Chem. C 2018, 122, 21724−21734

$$\frac{\lambda_B}{\sigma} = \frac{1}{4\pi\varepsilon}\frac{q^2}{\varepsilon_0 k_B T \sigma}$$

$$\frac{\lambda_D}{\sigma} = \sqrt{\frac{\varepsilon\varepsilon_0 k_B T}{\sigma^2 \sum_\pm n_\pm q_\pm^2}} = \sqrt{\frac{\varepsilon}{\frac{q^2}{\varepsilon_0 k_B T \sigma}}\frac{\pi}{6\phi}} = \frac{1}{2}\sqrt{\frac{\sigma}{\lambda_B}\frac{1}{6\phi}} \quad (16)$$

where $n_\pm$ and n_- is the number density of cations and anions, respectively, and $\phi = \frac{\pi}{6}\sigma^3(n_+ + n_-)$ is the volume fraction occupied by ions, each defined on the accessible region of width L. We fix $\phi = 0.375$ such that we obtain $\lambda_B/\sigma = 0.23$ and $\lambda_D/\sigma = 0.69$ for the (macro-)ions. Thus, both of the lengths, λ_B and λ_D, are smaller than the particle diameter σ, and a strong effect of the hard-sphere interactions is expected.

Quantities of Interest. At the start, the system is equilibrated without applied potential to reach a steady state, at which point the transverse oscillating voltage $U(t)$ is introduced. The latter causes an electric field $E(t)$ and thus an ion flux in z-direction. The resulting ion flux density $\vec{j}_{p,\pm}(\vec{r}, t)$ is a periodic function in time and can easily be derived from eq 1 together with the continuity equation $\frac{\partial \rho_\pm(\vec{r}, t)}{\partial t} = -\nabla\cdot\vec{j}_{p,\pm}(\vec{r}, t)$ as

$$\vec{j}_{p,\pm}(\vec{r}, t) = -\beta D\left[\rho_\pm(\vec{r}, t)\nabla\left(\frac{\delta\mathcal{F}[\rho_+(\vec{r}, t), \rho_-(\vec{r}, t)]}{\delta\rho_\pm(\vec{r}, t)}\right)\right] \quad (17)$$

The ionic current density in z-direction is then given as

$$j(\vec{r}, t) = \sum_\pm q_\pm \vec{j}_{p,\pm}(\vec{r}, t)\cdot\hat{e}_z \quad (18)$$

Analogously, we can define contributions to the ion flux density that stem from different energy terms

$$\vec{j}^{\,k}_{p,\pm}(\vec{r}, t) = -\beta D\left[\rho_\pm(\vec{r}, t)\nabla\left(\frac{\delta\mathcal{F}^k[\rho_+(\vec{r}, t), \rho_-(\vec{r}, t)]}{\delta\rho_\pm(\vec{r}, t)}\right)\right] \quad (19)$$

where $k \in \{\text{id, HS, Coul, ext}\}$ and the ionic current density contribution is then again given by eq 18 replacing $\vec{j}_{p,\pm}$ with $\vec{j}^{\,k}_{p,\pm}$. Note that considering the contributions due to the external potential, $\mathcal{F}^{\text{ext}}$, and the ideal term, $\mathcal{F}^{\text{id}}$, the equation is identical to the Nernst–Planck equation. Adding also the Coulomb interaction term, $\mathcal{F}^{\text{Coul}}$, we obtain the Poisson–Nernst–Planck (PNP) description. The additional hard-sphere interaction term, $\mathcal{F}^{\text{HS}}$, is a nontrivial extension to this model accounting for the finite ion size, an essential contribution due to the small system width.

The current response is nondimensionalized relative to $j_0 = e/\sigma^2\tau_0$ and can, due to its periodicity, be decomposed into different harmonic contributions of amplitude j_n with $n = 1, 2, 3, \ldots$ The harmonics are obtained as

$$j_n(\vec{r}) = \frac{2}{T}\int_{-T/2}^{T/2} \mathrm{d}t\, j(\vec{r}, t)\, \mathrm{e}^{-\mathrm{i}n\omega t} \quad (20)$$

with $T = 2\pi/\omega$. Plots of the current will always show j while we use j_1, the amplitude of the first harmonic of the current density, to define the complex impedance Z given by

$$\frac{Z}{Z_0} = U^*\frac{j_0}{j_1}\,\mathrm{e}^{\mathrm{i}(\phi_U - \phi_{j_1})} \quad (21)$$

The scale of this quantity is set by $z_0 = k_B T\tau_0/e^2$. Higher harmonic contributions to the current (j_n with $n \geq 2$) will be discussed in the Supporting Information.

RESULTS AND DISCUSSION

Density Profiles and Current Response. First, we investigate the effect of the system width on the density distribution and current induced in the system. In Figure 2, the effect of the hard-sphere interaction is reflected in the increased values of the particle densities at the walls and at multiples of σ. Counterion accumulation at the walls is enhanced with the application of a finite voltage difference and for larger system widths, when ions are attracted to walls of opposite charge. The effect is preserved but weakens as the frequency increases. Thus, lower frequencies correspond to higher amounts of localized ions at the walls. Further, while at high frequencies the current is harmonic and in phase with the driving voltage, the low-frequency current shows anharmonicity and a phase shift; see Figure 3. For a stronger electric field (smaller system width), the current becomes increasingly

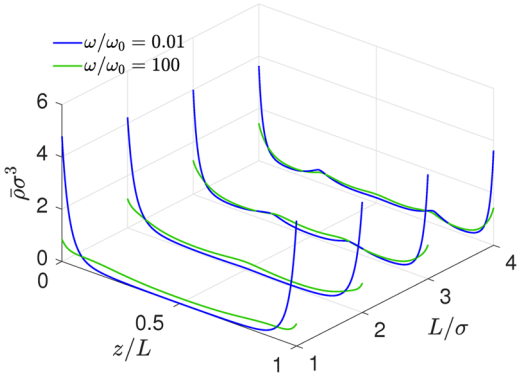

Figure 2. Mean density distribution $\bar{\rho} \equiv \bar{\rho}_+ = \bar{\rho}_-$ averaged over one period for different widths, $L/\sigma = 1$, $L/\sigma = 2$, $L/\sigma = 3$, and $L/\sigma = 4$. Layering at the walls and at multiples of σ is observed. The effect is stronger for smaller frequencies.

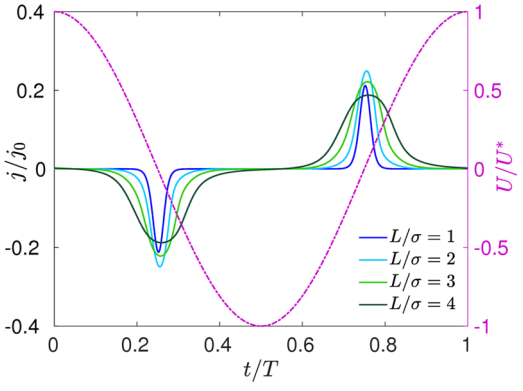

Figure 3. Time dependence of current density at the center position ($z = L/2$) at small frequency ($\omega/\omega_0 = 0.01$). The resulting current shows strong anharmonicity and a phase shift with respect to the driving voltage $U(t)$, which is also plotted for reference (purple dash-dot line).

DOI: 10.1021/acs.jpcc.8b05559
J. Phys. Chem. C 2018, 122, 21724–21734

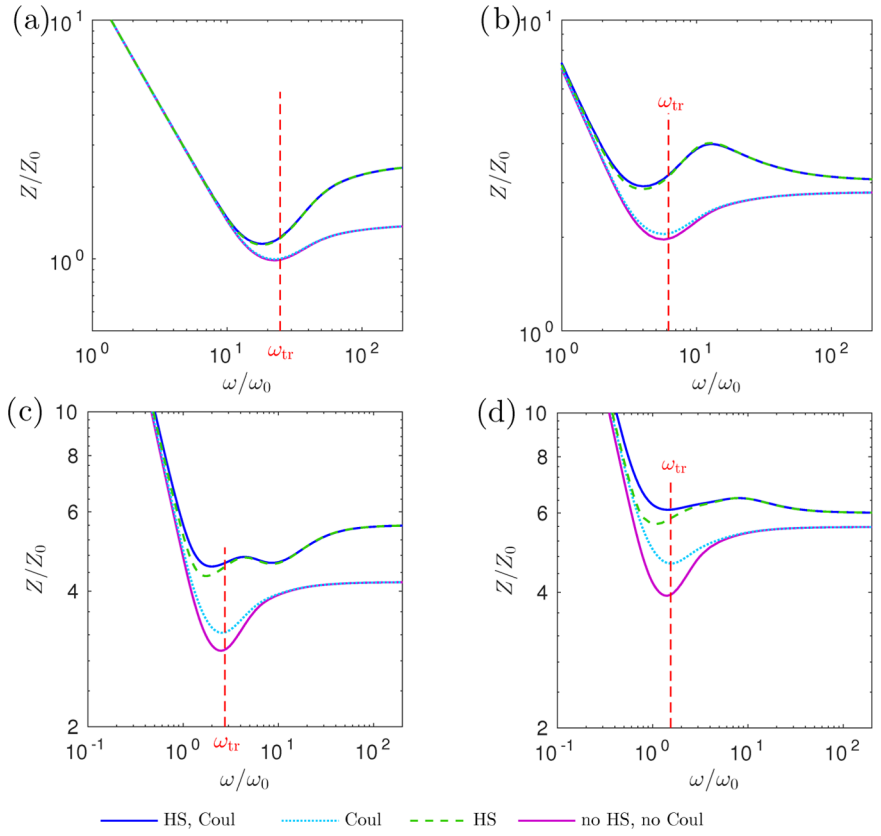

Figure 4. Impedance with respect to angular frequency of the driving voltage ω for systems of lengths (a) $L/\sigma = 1$, (b) $L/\sigma = 2$, (c) $L/\sigma = 3$, and (d) $L/\sigma = 4$. The impedance values in the large frequency limit are reached from below for system lengths that are odd multiples of σ and from above for even ones. The analytical result for the position of the minimum in the impedance ω_{tr} according to eq 14 is also indicated.

peaked and the system response is nonlinear. The effect of short-range electrostatic correlations on the density profile based on the usage of the more sophisticated density functional from ref 74 is discussed in the Supporting Information.

Impedance Response. To examine the effect of the hard-sphere character of the ions, eq 1 was solved, for reference, with and without hard-sphere (HS) and Coulomb (Coul) interaction terms, and the impedance corresponding to the ion flux at the capacitor midplane was calculated; see Figure 4. Hard-sphere interactions lead to a large increment of this impedance at medium and high frequencies, whereas the effect of Coulomb interactions in determining the impedance is much less pronounced.

The hard-sphere contribution is responsible for a maximum in the impedance at $\omega > \omega_{tr}$. This feature vanishes when the hard-sphere contribution is switched off. We conjecture that the maximum is thus related to the additional structure in the density distribution induced by hard-sphere interactions.

Another peculiar feature in Figure 4 is the impedance minimum seen at $\omega \approx \omega_0$. This feature is independent of the hard-sphere character of ions and also independent of their Coulomb interaction. It represents a resonance phenomenon that should be common to all systems of confined ions exposed to an oscillating external potential. While overdamped particles in a continuous environment do not show resonance behavior, it is the confinement in combination with the ion oscillation that leads to the resonance effect. However, observation of this phenomenon depends critically on system parameters. It is a peculiar signature of the pronounced wall effects, which prevail in strongly confined systems upon application of an AC voltage with large amplitude. Under normal conditions in planar capacitive devices, the resonance should be quenched by thermal diffusion.[38−40,50,54] Diffusion causes a melting or dephasing of the highly coherent ion motion induced by wall effects. Since the occurrence of the impedance resonance is not affected by hard-sphere or Coulombic interaction terms, the phenomenon can be illustrated and explained using a highly simplified model, which will be presented next.

Resonance Effect. *Single-Ion Capacitor Model.* The origin of the minimum in Figure 4 must be universal and can thus be understood for the simple case of a noninteracting gas of ions with charge q confined between two charged plates. For simplicity, we neglect thermal motion. In the non-interacting case, every ion can be considered individually. The equation of motion for each ion is equivalent to the case of a capacitor configuration with just one ion between the plates and is given by

$$\dot{z}(t) = \frac{qE_0}{\gamma}\cos(\omega t) \tag{22}$$

with the friction coefficient γ and the angular frequency ω. The ion position is then

$$z(t) = z_0 + \frac{qE_0}{\omega\gamma}\sin(\omega t) \tag{23}$$

with arbitrary starting position z_0. During one oscillation period, an ion will transfer through a total transverse distance $d_{tr} = 2qE_0/\omega\gamma$ between the plates.

DOI: 10.1021/acs.jpcc.8b05559
J. Phys. Chem. C 2018, 122, 21724−21734

In terms of the distance d_{tr} and frequency ω, we can distinguish three regimes. In the regime of small amplitude, $d_{tr} < L/2$, and high frequency, $\omega > 4qE_0/\gamma L$, ions that cross the midplane and contribute to j and Z at this plane perform full harmonic oscillations with zero phase shift to the applied AC voltage. The resulting ionic current density is easily obtained as

$$j(z = L/2, t) = q\dot{z}(t)\rho_0 = \frac{q^2E_0\rho_0}{\gamma}\cos(\omega t) \tag{24}$$

in the case of negligible thermal motion.

In the regime of large amplitude, $d_{tr} > L$, and small frequency, $\omega < 2qE_0/\gamma L$, all ions will accumulate at either one of the surface planes during a half-period. Therefore, under ideal conditions, as considered with this simple model, cations and anions will perform a highly coherent motion and cross the midplane as two condensed and oppositely directed layers; see also Figure 3. In this regime, all ions will contribute to current and impedance responses determined at this plane. The ionic current density, averaged over a half-period, will thus be proportional to the frequency of the applied field; it will be highly anharmonic and exhibit a monotonically decreasing phase shift with decreasing ω, approaching $-\frac{\pi}{2}$ in the zero frequency limit. The solutions of eq 22 in this and the following case are given in the Supporting Information.

In the intermediate regime with $L/2 \leq d_{tr} \leq L$ and $\frac{4qE_0}{\gamma L} \geq \omega \geq \frac{2qE_0}{\gamma L}$, all ions in the system contribute to current density and impedance at the midplane; however, a fraction d_{tr}/L of these ions forms a condensed layer at the walls, whereas the remaining fraction of ions remains distributed uniformly in between and follows the applied field harmonically and with zero phase shift. The transition that gives rise to the impedance resonance occurs at $\omega_{tr} = \frac{4qE_0}{\gamma L}$: slightly above this frequency, only 50% of ions (corresponding to d_{tr}/L) contribute to the ion flux at the midplane, and as the frequency increases, this fraction diminishes with the decrease of d_{tr}/L. In the frequency range at and below ω_{tr}, 100% of ions contribute to the midplane current as a consequence of the ion condensation at the walls. Thus, the resonance seen in Figure 4 has a simple geometric interpretation.

A necessary condition for observing this resonance at finite temperature is that diffusional dephasing of the coherent ion motion will take place on a time scale that is much larger than the ion transit time, that is, $\tau_{diff} \gg \tau_{tr}$ or $\omega_{diff} \ll \omega_{tr}$. The critical parameter that decides this condition is U^*, which should be much larger than 1 for the ion condensation effect to be discernible.

Further, the preceding small amplitude or high frequency case, eq 24, can be adopted to determine the high frequency limit behavior of nonuniform distributions of interacting particles by interpreting ρ as a local density, which we understand as the mean density over the length that particles oscillate, d_{tr}. Then, if the local density has a maximum at the plane of interest, j grows for smaller d_{tr}, that is, for larger ω, and the impedance $Z \propto 1/j$ declines toward its high frequency value. For a minimum in the density, the opposite is true and we approach the constant high-frequency impedance from below. This effect is also visible in Figure 4 for interacting particles (HS, Coul). For system lengths that are even multiples of σ, there is a maximum in the density at the center position when hard-sphere interactions are included and the high frequency limit of the impedance is approached from above. For odd multiples of σ, the center position is at a density minimum and the high frequency limit of the impedance is approached from below. Similarly, density inhomogeneities in the vicinity of the considered plane also appear in the impedance response at the corresponding frequencies, leading to additional extrema at medium frequencies.

Rescaled Resonance. We use the one-particle model to further investigate the emerging resonance. Defining the current averaged over a period of the driving signal $\bar{j} = \frac{1}{T}\int_0^T \mathrm{d}t j(t)$, we determine the corresponding time-averaged impedance $\tilde{Z} = \Delta U/\bar{j}\sigma^2$. For high frequencies, j is given by eq 24 in the athermal case. At finite temperature, we find that even though the condensed particles at the walls do not contribute to the current directly, diffusion from the condensed part into the gap center will lead to a density higher than the equilibrium density ρ_0 there. This effect is particularly dominant for medium frequencies where the fraction of condensed particles, d_{tr}/L, is expected to be high. As a next-order improvement, we correct for this effect by neglecting the peaked structure altogether. The numerical results for the density show that this is a valid approximation as the ion density peaks account for only about 10% of all ions. Considering only the uniform distribution part, the leftmost ions reach the extremal position d_{tr}, while the rightmost are pushed against the wall at position L. The effective width available to the ions is thus reduced to $L - d_{tr}$. The density, assuming again a constant distribution but now over the reduced region, is given by

$$\rho = \rho_0 L/(L - d_{tr}) \tag{25}$$

From eqs 24 and 25, we thus obtain

$$\bar{j} = \frac{2}{\pi}\frac{q^2E_0}{\gamma}\frac{\rho_0 L}{L - d_{tr}} \tag{26}$$

and the high frequency limit, $\omega \to \infty$, as $j^\infty = \frac{2}{\pi}\frac{q^2E_0\rho_0}{\gamma}$. Normalizing the frequencies to the transit frequency ω_{tr} and the impedance to the high frequency limit $Z^\infty = U^* j_0/j^\infty$, we find that the result is solely depending on the value of U^*; see Figure 5. An approximate analytic result in the limit of negligible thermal motion compared to the driving force is given by eq 26 for $\omega > \omega_{tr}$ and $\bar{j} = q\rho_0 L\omega/\pi$ for $\omega \leq \omega_{tr}$ when all ions are passing the midplane.

The resonance becomes more pronounced for higher values of U^*. However, it cannot exceed a factor of 2 between the resonance value and the high frequency limit of the impedance. High values of U^* may appear unphysical but could be realized by using multivalent ions rather than higher voltages.

Effect of Condensed Layer. *Impedance.* So far we have only considered the impedance corresponding to the current at the system center at $z = L/2$. However, it is intuitive to expect the local impedance response, that is, the impedance associated with the time-dependent current at a fixed point between the capacitor plates, to be highly dependent on the position. The current response in the ion layer at the wall should significantly differ from the current in the system center. As a next step, we therefore consider the dependence of the local impedance on the position between the two capacitor plates. In Figure 6, the case $z/\sigma = 2$ corresponds to the center of the system. The

DOI: 10.1021/acs.jpcc.8b05559
J. Phys. Chem. C 2018, 122, 21724−21734

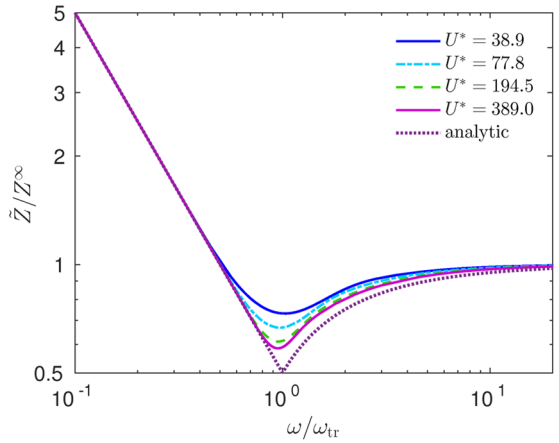

Figure 5. Impedance $\tilde{Z}$ for different values of the external voltage U^* and for the approximative analytic result with respect to angular frequency ω. The results are rescaled to the transition frequency ω_{tr} and the high frequency impedance limit Z^∞. The observed resonance at $\omega/\omega_{tr} = 1$ becomes more pronounced for higher U^*.

system response here is as expected, with a $1/\omega$ decay to the high frequency constant value in the impedance amplitude and the phase changing from $-\pi/2$ to 0. Approaching the wall, the position of $z/\sigma = 0.5$ corresponds to a density minimum and the large frequency limit of the impedance is approached from below. The rise in Z toward the high frequency limit is accompanied by a maximum in the phase with the system response even becoming inductive ($\varphi > 0$) for a limited frequency range. The phase behavior is caused by ion condensation at the wall. These ions lead to a temporal shift of the maximum in the current response toward the time at which they pass the plane. The resulting phase shift increases with ω and may even become positive. Upon further increasing ω, ions from the wall no longer reach the plane and the effect abates.

Decreasing the distance to the wall, we find that the low frequency phase value approaches zero as we enter the region of condensed ions. If we now consider again the time the ions condensed at the wall take to reach the plane at which we determine the impedance, we find that some of these ions are already present at the considered plane, reducing the phase shift toward zero. The effect becomes stronger the more ions are present at the plane, so the closer we are to the wall. At large frequencies, the oscillation amplitude is very small and the current is constituted by the ions freely oscillating in the field; thus, also in this limit the phase grows toward zero.

A discussion of the effect of short-range electrostatic correlations on the impedance response based on the usage of the more sophisticated density functional from ref 74 is included in the Supporting Information.

Current Components. To better understand the effect of ion interaction on the current, we separate the flow into contributions corresponding to the different energy terms in eq 2. In Figure 7, the flows caused by the external electric field, j_{el}, by the hard-sphere, j_{HS}, and Coulomb interaction, j_{Coul}, and the one due to diffusion of the ions, j_{diff}, are shown together with the total flow, j_{tot}, as a function of time for two different frequencies.

At the center (right column), the largest contribution to the total flow is always given by the flow due to the external electric field. Owing to the moderate density at this position, the hard-sphere interaction term is negligible. At high frequencies, the ions are freely following the electric field with a small amplitude oscillation around their position. The oscillation is in phase with the external electric field and the effect of the interaction terms is minute. For lower frequencies, however, the amplitude of the oscillatory motion becomes larger and the ions feel their neighbors via their Coulomb potential. Together with the diffusive flow, the Coulomb effect counteracts the particle oscillation induced by the electric field, resulting in a phase-shifted total flow j_{tot}.

Close to the wall, and at low frequencies, there are three main components that enter the total flow. These are given by hard-sphere interaction, diffusion, and external field term. The external electric field causes high densities near the walls for which the hard-sphere interaction becomes important. Additionally, the high-density gradient close to the walls causes a strong diffusive flow. The electric field and hard-sphere terms lead to charge flows in the same direction, pushing the ions against the wall. This flow is countered by the diffusive flow, which works against the formation of the accompanying density gradient. The different contributions show large anharmonicity, and the resulting current is tiny. At high frequencies, the current contributions are harmonic and the hard-sphere flow term is reduced due to the smaller oscillation amplitude.

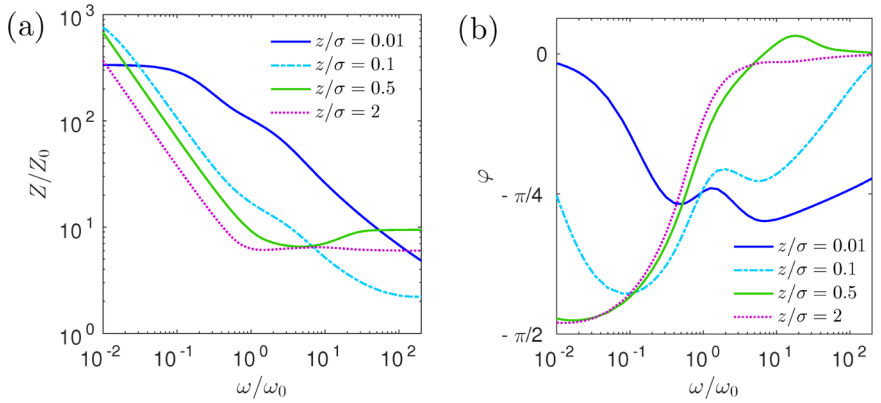

Figure 6. Impedance Z (a) and phase φ (b) as functions of frequency for different positions z between the plates. The frequency-dependent impedance changes qualitatively when approaching the wall. The parameters are $L/\sigma = 4$, $U^* = 38.9$.

DOI: 10.1021/acs.jpcc.8b05559
J. Phys. Chem. C 2018, 122, 21724−21734

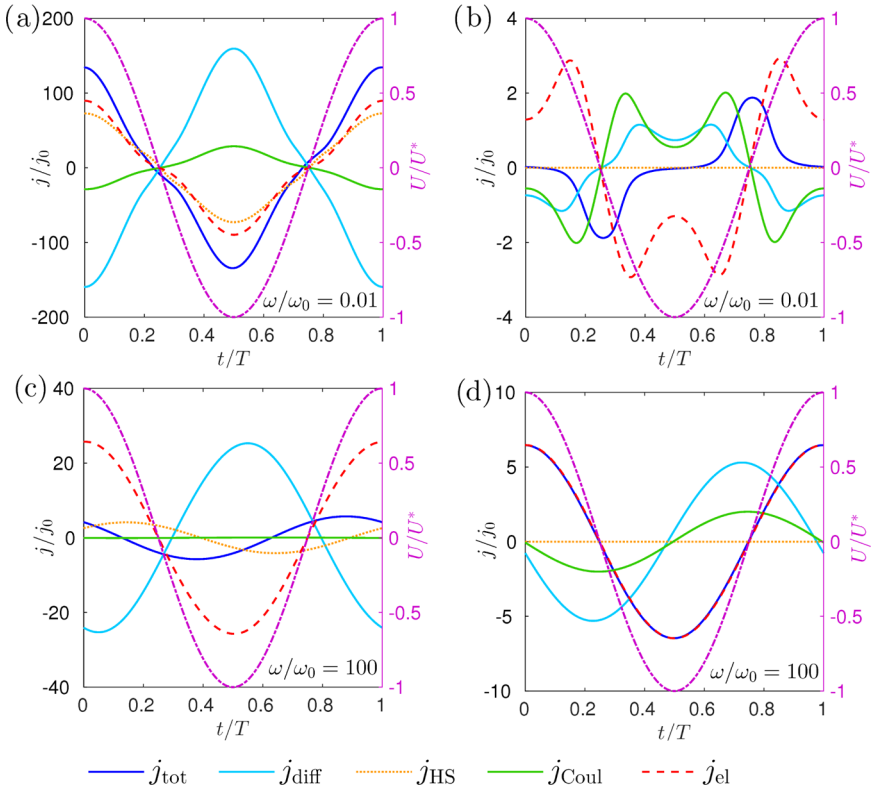

Figure 7. Contributions of the different flow terms to the system response for a system of length $L/\sigma = 4$ near the wall (a, c) ($z/\sigma = 0.01$) and at the center (b, d) ($z/\sigma = 2$). The contributions to the currents show considerable anharmonicity at small frequencies (upper row), which disappears at high frequencies (lower row). The effect of particle interaction grows for high densities close to the wall as well as for small frequencies. For better visibility, the current components have been scaled in (a) $j_{\rm tot} \times 1000$, $j_{\rm Coul} \times 10$, (b) $j_{\rm tot} \times 10$, and (d) $j_{\rm diff} \times 100$, $j_{\rm HS} \times 100$, $j_{\rm Coul} \times 100$. For reference, the voltage $U(t)$ is plotted against the right y axis.

CONCLUSIONS

We have explored by dynamic density functional theory the effect of an alternating voltage on a symmetric binary electrolyte confined between plan-parallel capacitor plates. This nonlinear theory provides a unifying framework to include steric interactions between ions and their drift dynamics induced by the AC electric field. It thus significantly generalizes previous approaches based on Poisson−Nernst−Planck theory. Besides the dynamical layering of the driven ions near the confining walls, we predict a resonance effect of the impedance, which can be traced back to a simple single-ion effect, but is modified by Coulomb and steric interactions. This effect becomes relevant in strong confinement and allows one to tune the electric response by confinement spacing, temperature, and external voltage applied. It was explored for two different realizations, both of vital importance to physical chemistry, namely, charged colloids and microions of nanometric size.

Future work should concentrate on the molecular details of the solvent as well as specific substrate properties like surface charges and roughness. In particular, reorientation and polarization effects of the liquid molecules and the impact of these effects on the capacitive ion response discussed here should be considered. Density functional theory can in fact be generalized toward solvent-ion mixtures[89,90] and more general external potentials. Modeling of electrode details can in principle be incorporated as well.

ASSOCIATED CONTENT

Supporting Information

The Supporting Information is available free of charge on the ACS Publications website at DOI: 10.1021/acs.jpcc.8b05559.

Comparison with modified functional from ref 74; current form for medium and low frequencies; contributions of higher harmonics in the current (PDF)

AUTHOR INFORMATION

Corresponding Author

*E-mail: hlowen@thphy.uni-duesseldorf.de. Phone: +49-211-81-11377. Fax: +49-211-81-10776.

ORCID

Sonja Babel: 0000-0002-7633-1493

Notes

The authors declare no competing financial interest.

ACKNOWLEDGMENTS

We thank Alexei A. Kornyshev and Andreas Härtel for helpful discussions. We gratefully acknowledge financial support by the DFG grant LO 418/19-1.

REFERENCES

(1) Jiang, D.-e.; Jin, Z.; Wu, J. Oscillation of Capacitance inside Nanopores. *Nano Lett.* **2011**, *11*, 5373−5377.

(2) Kornyshev, A. A. The Simplest Model of Charge Storage in Single File Metallic Nanopores. *Faraday Discuss.* **2013**, *164*, 117−133.

DOI: 10.1021/acs.jpcc.8b05559
J. Phys. Chem. C 2018, 122, 21724−21734

(3) Rochester, C. C.; Kondrat, S.; Pruessner, G.; Kornyshev, A. A. Charging Ultrananoporous Electrodes with Size-Asymmetric Ions Assisted by Apolar Solvent. *J. Phys. Chem. C* **2016**, *120*, 16042−16050.
(4) Kong, X.; Wu, J.; Henderson, D. Density Functional Theory Study of the Capacitance of Single File Ions in a Narrow Cylinder. *J. Colloid Interface Sci.* **2015**, *449*, 130−135.
(5) Leunissen, M. E.; Christova, C. G.; Hynninen, A.-P.; Royall, C. P.; Campbell, A. I.; Imhof, A.; Dijkstra, M.; van Roij, R.; van Blaaderen, A. Ionic Colloidal Crystals of Oppositely Charged Particles. *Nature* **2005**, *437*, 235−240.
(6) Demirörs, A. F.; Stiefelhagen, J. C. P.; Vissers, T.; Smallenburg, F.; Dijkstra, M.; Imhof, A.; van Blaaderen, A. Long-Ranged Oppositely Charged Interactions for Designing New Types of Colloidal Clusters. *Phys. Rev. X* **2015**, *5*, No. 021012.
(7) Würger, A. Transport in Charged Colloids Driven by Thermoelectricity. *Phys. Rev. Lett.* **2008**, *101*, No. 108302.
(8) Aricò, A. S.; Bruce, P.; Scrosati, B.; Tarascon, J.-M.; van Schalkwijk, W. Nanostructured Materials for Advanced Energy Conversion and Storage Devices. *Nat. Mater.* **2005**, *4*, 366−377.
(9) Montelongo, Y.; Sikdar, D.; Ma, Y.; McIntosh, A. J. S.; Velleman, L.; Kucernak, A. R.; Edel, J. B.; Kornyshev, A. A. Electrotunable Nanoplasmonic Liquid Mirror. *Nat. Mater.* **2017**, *16*, 1127−1135.
(10) Baughman, R. H.; Cui, C.; Zakhidov, A. A.; Iqbal, Z.; Barisci, J. N.; Spinks, G. M.; Wallace, G. G.; Mazzoldi, A.; De Rossi, D.; Rinzler, A. G.; et al. Carbon Nanotube Actuators. *Science* **1999**, *284*, 1340−1344.
(11) Kornyshev, A. A.; Twidale, R. M.; Kolomeisky, A. B. Current-Generating Double-Layer Shoe with a Porous Sole: Ion Transport Matters. *J. Phys. Chem. C* **2017**, *121*, 7584−7595.
(12) Porada, S.; Zhao, R.; van der Wal, A.; Presser, V.; Biesheuvel, P. Review on the Science and Technology of Water Desalination by Capacitive Deionization. *Prog. Mater. Sci.* **2013**, *58*, 1388−1442.
(13) Biesheuvel, P. M.; Bazant, M. Z. Nonlinear Dynamics of Capacitive Charging and Desalination by Porous Electrodes. *Phys. Rev. E* **2010**, *81*, No. 031502.
(14) Härtel, A.; Janssen, M.; Samin, S.; van Roij, R. Fundamental Measure Theory for the Electric Double Layer: Implications for Blue-Energy Harvesting and Water Desalination. *J. Phys.: Condens. Matter* **2015**, *27*, No. 194129.
(15) Evans, R.; Oettel, M.; Roth, R.; Kahl, G. New Developments in Classical Density Functional Theory. *J. Phys.: Condens. Matter* **2016**, *28*, No. 240401.
(16) Archer, A. J.; Evans, R. Dynamical Density Functional Theory and Its Application to Spinodal Decomposition. *J. Chem. Phys.* **2004**, *121*, 4246−4254.
(17) Español, P.; Löwen, H. Derivation of Dynamical Density Functional Theory Using the Projection Operator Technique. *J. Chem. Phys.* **2009**, *131*, No. 244101.
(18) Marconi, U. M. B.; Tarazona, P. Dynamic Density Functional Theory of Fluids. *J. Chem. Phys.* **1999**, *110*, 8032−8044.
(19) Royall, C. P.; Leunissen, M. E.; van Blaaderen, A. A New Colloidal Model System to Study Long-Range Interactions Quantitatively in Real Space. *J. Phys.: Condens. Matter* **2003**, *15*, S3581−S3596.
(20) Vissers, T.; Wysocki, A.; Rex, M.; Lowen, H.; Royall, C. P.; Imhof, A.; van Blaaderen, A. Lane Formation in Driven Mixtures of Oppositely Charged Colloids. *Soft Matter* **2011**, *7*, 2352−2356.
(21) Vissers, T.; van Blaaderen, A.; Imhof, A. Band Formation in Mixtures of Oppositely Charged Colloids Driven by an ac Electric Field. *Phys. Rev. Lett.* **2011**, *106*, No. 228303.
(22) Saunders, B. R.; Vincent, B. Microgel Particles as Model Colloids: Theory, Properties and Applications. *Adv. Colloid Interface Sci.* **1999**, *80*, 1−25.
(23) Holmqvist, P.; Mohanty, P. S.; Nägele, G.; Schurtenberger, P.; Heinen, M. Structure and Dynamics of Loosely Cross-Linked Ionic Microgel Dispersions in the Fluid Regime. *Phys. Rev. Lett.* **2012**, *109*, No. 048302.
(24) Lemay, S. G.; Kang, S.; Mathwig, K.; Singh, P. S. Single-Molecule Electrochemistry. *Acc. Chem. Res.* **2013**, *46*, 369−377.
(25) Catalano, J.; Biesheuvel, P. AC-Driven Electro-Osmotic Flow in Charged Nanopores 2018, arXiv:1805.10845. arXiv.org e-Printarchive. https://arxiv.org/abs/1805.10845 (accessed May 28, 2018).
(26) Gouy, M. Sur la Constitution de la Charge Electrique à la Surface d'un Electrolyte. *J. Phys. Theor. Appl.* **1910**, *9*, 457−468.
(27) Chapman, D. L. LI. A Contribution to the Theory of Electrocapillarity. *London, Edinburgh Dublin Philos. Mag. J. Sci.* **1913**, *25*, 475−481.
(28) Bikerman, J. XXXIX. Structure and Capacity of Electrical Double Layer. *London, Edinburgh Dublin Philos. Mag. J. Sci.* **1942**, *33*, 384−397.
(29) Borukhov, I.; Andelman, D.; Orland, H. Steric Effects in Electrolytes: A Modified Poisson-Boltzmann Equation. *Phys. Rev. Lett.* **1997**, *79*, 435−438.
(30) Kornyshev, A. A. Double-Layer in Ionic Liquids: Paradigm Change? *J. Phys. Chem. B* **2007**, *111*, 5545−5557.
(31) Burger, M.; Schlake, B.; Wolfram, M.-T. Nonlinear Poisson-Nernst-Planck Equations for Ion Flux through Confined Geometries. *Nonlinearity* **2012**, *25*, 961−990.
(32) Siddiqua, F.; Wang, Z.; Zhou, S. A Modified Poisson-Nernst-Planck Model with Excluded Volume Effect: Theory and Numerical Implementation 2017, arxiv:1801.00751. arXiv.org e-Printarchive. https://arxiv.org/abs/1801.00751 (accessed Nov 2, 2013).
(33) Meng, D.; Zheng, B.; Lin, G.; Sushko, M. L. Numerical Solution of 3D Poisson-Nernst-Planck Equations Coupled with Classical Density Functional Theory for Modeling Ion and Electron Transport in a Confined Environment. *Commun. Comput. Phys.* **2014**, *16*, 1298−1322.
(34) Qiao, Y.; Liu, X.; Chen, M.; Lu, B. A Local Approximation of Fundamental Measure Theory Incorporated into Three Dimensional Poisson-Nernst-Planck Equations to Account for Hard Sphere Repulsion Among Ions. *J. Stat. Phys.* **2016**, *163*, 156−174.
(35) Jiang, J.; Cao, D.; en Jiang, D.; Wu, J. Time-Dependent Density Functional Theory for Ion Diffusion in Electrochemical Systems. *J. Phys.: Condens. Matter* **2014**, *26*, No. 284102.
(36) Lian, C.; Zhao, S.; Liu, H.; Wu, J. Time-Dependent Density Functional Theory for the Charging Kinetics of Electric Double Layer Containing Room-Temperature Ionic Liquids. *J. Chem. Phys.* **2016**, *145*, No. 204707.
(37) Gongadze, E.; Iglič, A. Asymmetric Size of Ions and Orientational Ordering of Water Dipoles in Electric Double Layer Model - an Analytical Mean-Field Approach. *Electrochim. Acta* **2015**, *178*, 541−545.
(38) Beunis, F.; Strubbe, F.; Marescaux, M.; Beeckman, J.; Neyts, K.; Verschueren, A. R. M. Dynamics of Charge Transport in Planar Devices. *Phys. Rev. E* **2008**, *78*, No. 011502.
(39) Olesen, L. H.; Bazant, M. Z.; Bruus, H. Strongly Nonlinear Dynamics of Electrolytes in Large AC Voltages. *Phys. Rev. E* **2010**, *82*, No. 011501.
(40) Feicht, S. E.; Frankel, A. E.; Khair, A. S. Discharging Dynamics in an Electrolytic Cell. *Phys. Rev. E* **2016**, *94*, No. 012601.
(41) Levin, Y. Electrostatic Correlations: From Plasma to Biology. *Rep. Prog. Phys.* **2002**, *65*, 1577−1632.
(42) Fisher, M. E.; Levin, Y. Criticality in Ionic Fluids: Debye-Hückel Theory, Bjerrum, and Beyond. *Phys. Rev. Lett.* **1993**, *71*, 3826−3829.
(43) van Roij, R.; Hansen, J.-P. Van der Waals−Like Instability in Suspensions of Mutually Repelling Charged Colloids. *Phys. Rev. Lett.* **1997**, *79*, 3082−3085.
(44) Kornyshev, A. A.; Vilfan, I. Phase Transitions at the Electrochemical Interface. *Electrochim. Acta* **1995**, *40*, 109−127.
(45) Kornyshev, A. A.; Qiao, R. Three-Dimensional Double Layers. *J. Phys. Chem. C* **2014**, *118*, 18285−18290.
(46) Messina, R.; Holm, C.; Kremer, K. Strong Attraction between Charged Spheres due to Metastable Ionized States. *Phys. Rev. Lett.* **2000**, *85*, 872−875.

DOI: 10.1021/acs.jpcc.8b05559
J. Phys. Chem. C 2018, 122, 21724−21734

(47) Lobaskin, V.; Dünweg, B.; Medebach, M.; Palberg, T.; Holm, C. Electrophoresis of Colloidal Dispersions in the Low-Salt Regime. *Phys. Rev. Lett.* **2007**, *98*, No. 176105.
(48) Fennell, C. J.; Bizjak, A.; Vlachy, V.; Dill, K. A. Ion Pairing in Molecular Simulations of Aqueous Alkali Halide Solutions. *J. Phys. Chem. B* **2009**, *113*, 6782−6791.
(49) Girotto, M.; dos Santos, A. P.; Levin, Y. Simulations of Ionic Liquids Confined by Metal Electrodes Using Periodic Green Functions. *J. Chem. Phys.* **2017**, *147*, No. 074109.
(50) Bazant, M. Z.; Thornton, K.; Ajdari, A. Diffuse-Charge Dynamics in Electrochemical Systems. *Phys. Rev. E* **2004**, *70*, No. 021506.
(51) Bazant, M. Z.; Kilic, M. S.; Storey, B. D.; Ajdari, A. Towards an Understanding of Induced-Charge Electrokinetics at Large Applied Voltages in Concentrated Solutions. *Adv. Colloid Interface Sci.* **2009**, *152*, 48−88.
(52) Härtel, A.; Kohl, M.; Schmiedeberg, M. Anisotropic Pair Correlations in Binary and Multicomponent Hard-Sphere Mixtures in the Vicinity of a Hard Wall: A Combined Density Functional Theory and Simulation Study. *Phys. Rev. E* **2015**, *92*, No. 042310.
(53) Härtel, A.; Samin, S.; van Roij, R. Dense Ionic Fluids Confined in Planar Capacitors: On- and Out-of-Plane Structure from Classical Density Functional Theory. *J. Phys.: Condens. Matter* **2016**, *28*, No. 244007.
(54) Härtel, A. Structure of Electric Double Layers in Capacitive Systems and to what Extent (Classical) Density Functional Theory Describes It. *J. Phys.: Condens. Matter* **2017**, *29*, No. 423002.
(55) Gillespie, D. A Review of Steric Interactions of ions: Why Some Theories Succeed and Others Fail to Account for Ion Size. *Microfluid. Nanofluid.* **2015**, *18*, 717−738.
(56) Härtel, A.; Janssen, M.; Weingarth, D.; Presser, V.; van Roij, R. Heat-to-Current Conversion of Low-Grade Heat from a Thermocapacitive Cycle by Supercapacitors. *Energy Environ. Sci.* **2015**, *8*, 2396−2401.
(57) Orkoulas, G.; Panagiotopoulos, A. Z. Phase behavior of the Restricted Primitive Model and Square-Well Fluids from Monte Carlo Simulations in the Grand Canonical Ensemble. *J. Chem. Phys.* **1999**, *110*, 1581−1590.
(58) Luijten, E.; Fisher, M. E.; Panagiotopoulos, A. Z. Universality Class of Criticality in the Restricted Primitive Model Electrolyte. *Phys. Rev. Lett.* **2002**, *88*, No. 185701.
(59) Yan, Q.; de Pablo, J. J. Hyper-Parallel Tempering Monte Carlo: Application to the Lennard-Jones Fluid and the Restricted Primitive Model. *J. Chem. Phys.* **1999**, *111*, 9509−9516.
(60) Hynninen, A.-P.; Leunissen, M. E.; van Blaaderen, A.; Dijkstra, M. CuAu Structure in the Restricted Primitive Model and Oppositely Charged Colloids. *Phys. Rev. Lett.* **2006**, *96*, No. 018303.
(61) Panagiotopoulos, A. Z. Critical Parameters of the Restricted Primitive Model. *J. Chem. Phys.* **2002**, *116*, 3007−3011.
(62) Caillol, J.-M.; Levesque, D.; Weis, J.-J. Critical Behavior of the Restricted Primitive Model Revisited. *J. Chem. Phys.* **2002**, *116*, 10794−10800.
(63) Valleau, J.; Torrie, G. Heat Capacity of the Restricted Primitive Model near Criticality. *J. Chem. Phys.* **1998**, *108*, 5169−5172.
(64) de Carvalho, R. J. F. L.; Evans, R. Criticality of Ionic Fields: The Ginzburg Criterion for the Restricted Primitive Model. *J. Phys.: Condens. Matter* **1995**, *7*, L575−L583.
(65) Smit, B.; Esselink, K.; Frenkel, D. Solid-Solid and Liquid-Solid Phase Equilibria for the Restricted Primitive Model. *Mol. Phys.* **1996**, *87*, 159−166.
(66) Alts, T.; Nielaba, P.; D'Aguanno, B.; Forstmann, F. A Local Density Functional Approximation for the Ion Distribution Near a Charged Electrode in the Restricted Primitive Model Electrolyte. *Chem. Phys.* **1987**, *111*, 223−240.
(67) Hansen, J.-P.; Löwen, H. Effective Interactions Between Electric Double Layers. *Annu. Rev. Phys. Chem.* **2000**, *51*, 209−242.
(68) Evans, R. The Nature of the Liquid-Vapour Interface and Other Topics in the Statistical Mechanics of Non-Uniform, Classical Fluids. *Adv. Phys.* **1979**, *28*, 143−200.
(69) Gillespie, D.; Nonner, W.; Eisenberg, R. S. Coupling Poisson-Nernst-Planck and Density Functional Theory to Calculate Ion Flux. *J. Phys.: Condens. Matter* **2002**, *14*, 12129.
(70) Gillespie, D.; Nonner, W.; Eisenberg, R. S. Density Functional Theory of Charged, Hard-Sphere Fluids. *Phys. Rev. E* **2003**, *68*, No. 031503.
(71) Gillespie, D.; Valiskó, M.; Boda, D. Density Functional Theory of the Electrical Double Layer: The RFD Functional. *J. Phys.: Condens. Matter* **2005**, *17*, 6609−6626.
(72) Gillespie, D. Free-Energy Density Functional of Ions at a Dielectric Interface. *J. Phys. Chem. Lett.* **2011**, *2*, 1178−1182.
(73) Roth, R.; Gillespie, D. Physics of Size Selectivity. *Phys. Rev. Lett.* **2005**, *95*, No. 247801.
(74) Roth, R.; Gillespie, D. Shells of Charge: A Density Functional Theory for Charged Hard Spheres. *J. Phys.: Condens. Matter* **2016**, *28*, No. 244006.
(75) Patra, C. N.; Ghosh, S. K. A Nonlocal Density Functional Theory of Electric Double Layer: Symmetric Electrolytes. *J. Chem. Phys.* **1994**, *100*, 5219−5229.
(76) Patra, C. N.; Ghosh, S. K. A Nonlocal Density-Functional Theory of Electric Double Layer: Charge-Asymmetric Electrolytes. *J. Chem. Phys.* **1994**, *101*, 4143−4149.
(77) Patra, C. N.; Ghosh, S. K. Density functional Approach to the Structure of Uniform Fluids. *J. Chem. Phys.* **1997**, *106*, 2762−2770.
(78) Patra, C. N.; Yethiraj, A. Density Functional Theory for the Distribution of Small Ions around Polyions. *J. Phys. Chem. B* **1999**, *103*, 6080−6087.
(79) Kierlik, E.; Rosinberg, M. L. Density-Functional Theory for Inhomogeneous Fluids: Adsorption of Binary Mixtures. *Phys. Rev. A* **1991**, *44*, 5025−5037.
(80) Hansen, J.; McDonald, I. *Theory of Simple Liquids*; Elsevier Science, 2006.
(81) Lipkowitz, K.; Boyd, D. *Reviews in Computational Chemistry*; Wiley, 2009.
(82) Tarazona, P. Density Functional for Hard Sphere Crystals: A Fundamental Measure Approach. *Phys. Rev. Lett.* **2000**, *84*, 694−697.
(83) Rosenfeld, Y. Free-Energy Model for the Inhomogeneous Hard-Sphere Fluid Mixture and Density-Functional Theory of Freezing. *Phys. Rev. Lett.* **1989**, *63*, 980−983.
(84) Roth, R. Fundamental Measure Theory for Hard-Sphere Mixtures: A Review. *J. Phys.: Condens. Matter* **2010**, *22*, No. 063102.
(85) Härtel, A. *Density Functional Theory of Hard Colloidal Particles: From Bulk to Interfaces*; Shaker: Aachen, 2013.
(86) Oettel, M.; Görig, S.; Härtel, A.; Löwen, H.; Radu, M.; Schilling, T. Free Energies, Vacancy Concentrations, and Density Distribution Anisotropies in Hard-Sphere Crystals: A Combined Density Functional and Simulation Study. *Phys. Rev. E* **2010**, *82*, No. 051404.
(87) Tyldesley, J. *An Introduction to Tensor Analysis for Engineers and Applied Scientists*; Longman, 1975.
(88) Chaudhuri, M.; Allahyarov, E.; Löwen, H.; Egelhaaf, S. U.; Weitz, D. A. Triple Junction at the Triple Point Resolved on the Individual Particle Level. *Phys. Rev. Lett.* **2017**, *119*, No. 128001.
(89) Oleksy, A.; Hansen, J.-P. Microscopic Density Functional Theory of Wetting and Drying of a Solid Substrate by an Explicit Solvent Model of Ionic Solutions. *Mol. Phys.* **2009**, *107*, 2609−2624.
(90) Medasani, B.; Ovanesyan, Z.; Thomas, D. G.; Sushko, M. L.; Marucho, M. Ionic Asymmetry and Solvent Excluded Volume Effects on Spherical Electric Double Layers: A Density Functional Approach. *J. Chem. Phys.* **2014**, *140*, No. 204510.

DOI: 10.1021/acs.jpcc.8b05559
J. Phys. Chem. C 2018, 122, 21724−21734